

Cavity-Enhanced Near-Infrared Organic Photodetectors Based on a  
Conjugated Polymer Containing [1,2,5]Selenadiazolo[3,4-c]Pyridine

Peer-reviewed author version

Yang, Jinjin; Huang, Jun; Li, Ruiming; Li, Hui; Sun, Bin; Lin, Qianqian; Wang, Ming;  
Ma, Zaifei; VANDEWAL, Koen & Tang, Zheng (2021) Cavity-Enhanced  
Near-Infrared Organic Photodetectors Based on a Conjugated Polymer Containing  
[1,2,5]Selenadiazolo[3,4-c]Pyridine. In: Chemistry of Materials, 33 (13) , p. 5147 -5155.

DOI: 10.1021/acs.chemmater.1c01196

Handle: <http://hdl.handle.net/1942/34728>

# Cavity-Enhanced Near-Infrared Organic Photodetectors Based on A Conjugated Polymer Containing [1,2,5]Selenadiazolo[3,4-c]pyridine

Jinjin Yang,<sup>†</sup> Jun Huang,<sup>\*,†</sup> Ruiming Li,<sup>§</sup> Hui Li,<sup>†</sup> Bin Sun,<sup>†</sup> Qianqian Lin,<sup>§</sup> Ming Wang,<sup>†</sup> Zaifei Ma,<sup>\*,†</sup> Koen Vandewal,<sup>‡</sup> and Zheng Tang<sup>\*,†</sup>

<sup>†</sup> State Key Laboratory for Modification of Chemical Fibers and Polymer Materials, Center for Advanced Low-dimension Materials, College of Materials Science and Engineering, Donghua University, Shanghai 201620, China

<sup>§</sup> Key Lab of Artificial Micro- and Nano-structures of Ministry of Education of China, School of Physics and Technology, Wuhan University, Wuhan 430072, China

<sup>‡</sup> Institute for Materials Research (IMO-IMOMEC), Hasselt University, Wetenschapspark 1, B-3590 Diepenbeek, Belgium

Email: [ztang@dhu.edu.cn](mailto:ztang@dhu.edu.cn); [huangj@dhu.edu.cn](mailto:huangj@dhu.edu.cn); [mazaifei@dhu.edu.cn](mailto:mazaifei@dhu.edu.cn);

---

**ABSTRACT:** Miniaturization of spectrometers can be achieved using an array of narrowband photodetectors responsive at specific wavelengths. In this work, sensitive organic narrowband photodetectors with tunable spectral response in the near-infrared (NIR) wavelength range are demonstrated. This is achieved by using a resonant optical cavity device architecture based on a thick ZnO spacer to increase the weak NIR absorption of a low-bandgap conjugated polymer containing [1,2,5]selenadiazolo[3,4-c]pyridine. We realize spectral response full-width at half-maximum (FWHM) values down to 22 nm and calculated peak specific detectivity ( $D^*$ ) over  $10^{11}$  Jones in these cavity-enhanced photodetectors. More importantly, we achieve continuously tuned detection wavelengths over a wide wavelength range of 660–1510 nm. This allows for a proof-of-concept demonstration of a miniaturized spectrometer for the NIR wavelength range, able to resolve the NIR characteristic absorption bands of water, ethanol and acetone.

---

## INTRODUCTION

Optical spectrometers are instruments capable of measuring properties of light as a function of photon energy, and they are commonly used in medical diagnosis, environmental monitoring, and surveillance, etc.<sup>1,2</sup> Typical spectrometers are constructed by combining a broadband response photodetector with an additional moving optical component, i.e., dichroic prism or diffraction grating.<sup>1</sup> However, the use of the optical component increases the structural complexity and cost of the spectrometer, limiting the application of the device for more demanding areas such as consumer electronics.

Miniaturization of the spectrometer can be achieved using an array of narrowband photodetectors responsive at specific wavelengths. For inorganic materials based photodetectors, narrowband photodetection is normally achieved using expensive optical filters. Therefore, the cost of the mini-spectrometers based on such a device concept is high, especially for those operating in the near-infrared (NIR) wavelengths range (requiring the use of low-bandgap

semiconductors, such as InGaAs, Ge, etc). In this regard, organic semiconductors<sup>3</sup> are promising candidates for constructing NIR and narrowband photodetectors, because of their wide variety of optical and electrical properties and low materials cost.<sup>4-6</sup>

Through the tailored design of the organic photoactive materials, spectral selectivity and high responsivity in the ultra-violet and visible wavelength regions have been achieved using organic photodetectors, and full-width at half-maximum (FWHM) values of the response spectra in the range of 30–200 nm were reported.<sup>7-11</sup> In the NIR spectral region, narrowband organic photodetectors were constructed by exploiting the charge collection narrowing (CCN) effect: The use of the thick organic active layers results in the collection of charge carriers generated by absorbing photon energy at the optical bandgap.<sup>12-14</sup> Using this method however, the tunability of the spectral response is limited.

An approach to achieve a spectral response tunable over a broad wavelength range is to incorporate organic

semiconductors into a Fabry-Perot cavity device architecture.<sup>15–24</sup> To obtain a high spectral selectivity, the optical depth (absorption coefficient times thickness) of the photon-active layer sandwiched in between the two mirrors needs to be small. However, the typically very high absorption coefficients of the organic semiconductor (considered for organic photovoltaics or photodetectors) are too high to allow narrowband enhancement when incorporated as a 100 nm thin film in a cavity device architecture. Therefore, the active layers have to be ultra-thin, as demonstrated in vacuum-deposited organic cavity photodetectors based on 3–10 nm thick active layers: Tunable narrow-band spectral response in the visible wavelength range was realized.<sup>24</sup> For the near-infrared range, the weak absorption of the intermolecular charge-transfer (CT) states<sup>25,26</sup> formed in the donor/acceptor (D/A) blends have been enhanced by incorporating them in a cavity device architecture.<sup>23,27,28</sup> However, the absorption of CT states in organic blends is too weak to achieve sufficiently high photovoltaic external quantum efficiencies (EQEs). This led to a limited device responsivity in the NIR photodetectors with cavity-enhanced CT absorption.<sup>23,25,28,29</sup> Thus, the current challenge to explore the full potential of the miniaturized spectrometer concept based on the use of organic absorbers is to achieve spectroscopic photodetection for the NIR wavelengths.

In this work, a low-bandgap polymer, poly{[(4,4-dihexadecyl-4*H*-cyclopenta[2,1-*b*:3,4-*b'*] dithiophene-2,6-diyl)-alt-[4,4'-(4,4-dihexadecyl-4*H*-cyclopenta[1,2-*b*:5,4-*b'*] dithiophene-2,6-diyl) bis ([1,2,5]selenadiazolo[3,4-*c*] pyridine)-7,7'-diyl]} (PCDTPTSe) is synthesized. Combined with PC<sub>71</sub>BM, this material has the appropriate optical depth in 100–350 nm thin films to achieve narrowband cavity enhancement in the NIR spectral range 660–1510 nm. We realize FWHM values down to 22 nm and we achieve calculated peak specific detectivity ( $D^*$ ) on the order of  $10^{11}$  Jones, and measured  $D^*$  over  $10^{10}$  Jones, which is significantly better than previously reported organic cavity photodetectors based on enhanced CT state absorption.<sup>23,28</sup> In fact, the calculated  $D^*$  of the narrowband cavity photodetectors reported in this work is already comparable to that of some of the commercial Ge or PbS photodetectors, operating in a similar wavelength range.<sup>30,31</sup> Finally, a prototype miniaturized NIR spectrometer for the wavelength range of 660–1600 nm is successfully constructed to demonstrate the high potential of these low bandgap polymers combined with simple device architectures for low-cost NIR spectroscopic sensing applications.

## RESULTS AND DISCUSSION

A schematic picture of the device architecture used in this work is shown in Figure 1a. The photoactive layer is sandwiched in between two reflective electrodes, and the thickness of the front semitransparent electrode (Au, 30 nm) is optimized via optical transfer matrix (TM) simulations to ensure maximum absorption at the resonance wavelength.<sup>32</sup> The thicknesses of the ZnO and the MoO<sub>3</sub>

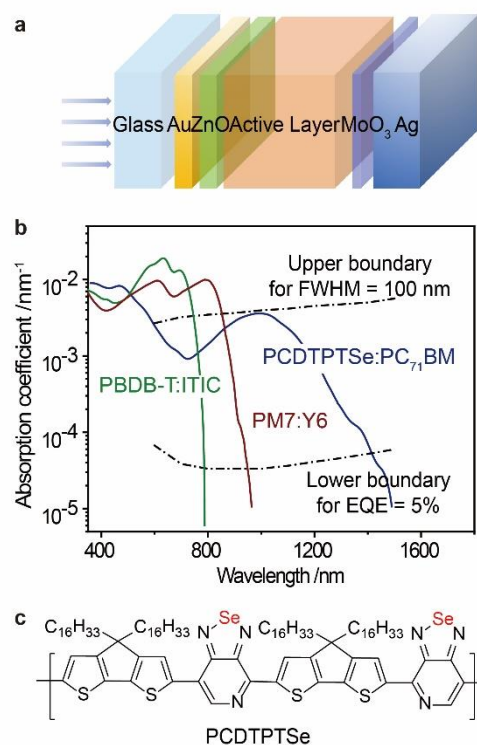


Figure 1 (a) Schematic for the device architecture of a resonant-cavity-enhanced organic photodetector. The thickness of the semitransparent Au electrode is 30 nm to allow for a highly efficient light in-coupling at the resonance wavelength and the thickness of the rear Ag electrode is 120 nm. The resonance wavelength can be tuned by varying the active layer thickness or the thicknesses of the interlayers. (b) Absorption coefficients of PBDB-T:ITIC and PM7:Y6, commonly used in organic optoelectronic devices, and absorption coefficient of PCDTPTSe:PC<sub>71</sub>BM used in this work. The estimated upper boundaries for the absorption coefficient indicating an FWHM of 100 nm and an EQE of 5% are shown in the plot, and they are derived using TM simulations. (c) Chemical structure of PCDTPTSe.

interlayers are 30 nm and 10 nm, respectively, unless stated otherwise. For such a cavity device, the resonance wavelength is proportional to the cavity thickness and the effective refractive indices of the layers in between the reflecting electrodes.<sup>20</sup> The FWHM value of the spectral response peak and the responsivity at the resonance wavelength are strongly related to the absorption coefficient of the active layer, the interlayers, and the reflective electrodes of the cavity photodetector: To realize a high resonant cavity effect and a small FWHM value, the absorption coefficients of all the materials used must be sufficiently low.<sup>20</sup> However, the low absorption coefficient of the active layer could lead to a low photodetector responsivity due to parasitic absorption losses in the interlayers or the electrodes. Therefore, a tradeoff between the spectral selectivity and responsivity exists. To evaluate the dependence of FWHM and EQE on the active layer absorption coefficient, TM simulations are performed for a hypothetical cavity photodetector based on the device architecture illustrated in Figure 1a. As shown in Figure 1b,

we find that to achieve an FWHM value smaller than 100 nm and EQE higher than 5%, the absorption coefficient of the active layer needs to be approximately in the range between  $10^{-3}$  and  $10^{-5}$   $\text{nm}^{-1}$ . Details regarding the TM simulation are provided in Supporting Information (SI, SI-2).

Typical organic D/A blends, such as PBDB-T:ITIC and PM7:Y6,<sup>33,34</sup> have rather narrow absorption bands and too high absorption coefficients (Figure 1b) preventing

sufficiently small FWHM values when incorporated into a cavity device architecture. In order to achieve a high spectral resolution (FWHM  $\ll 100$  nm) and tunability over a broad wavelength range, a material with a lower, broad, and featureless absorption coefficient is required. Furthermore, since recognition of compounds often relies on their specific spectral fingerprint in the NIR, extension to NIR wavelengths is desired.

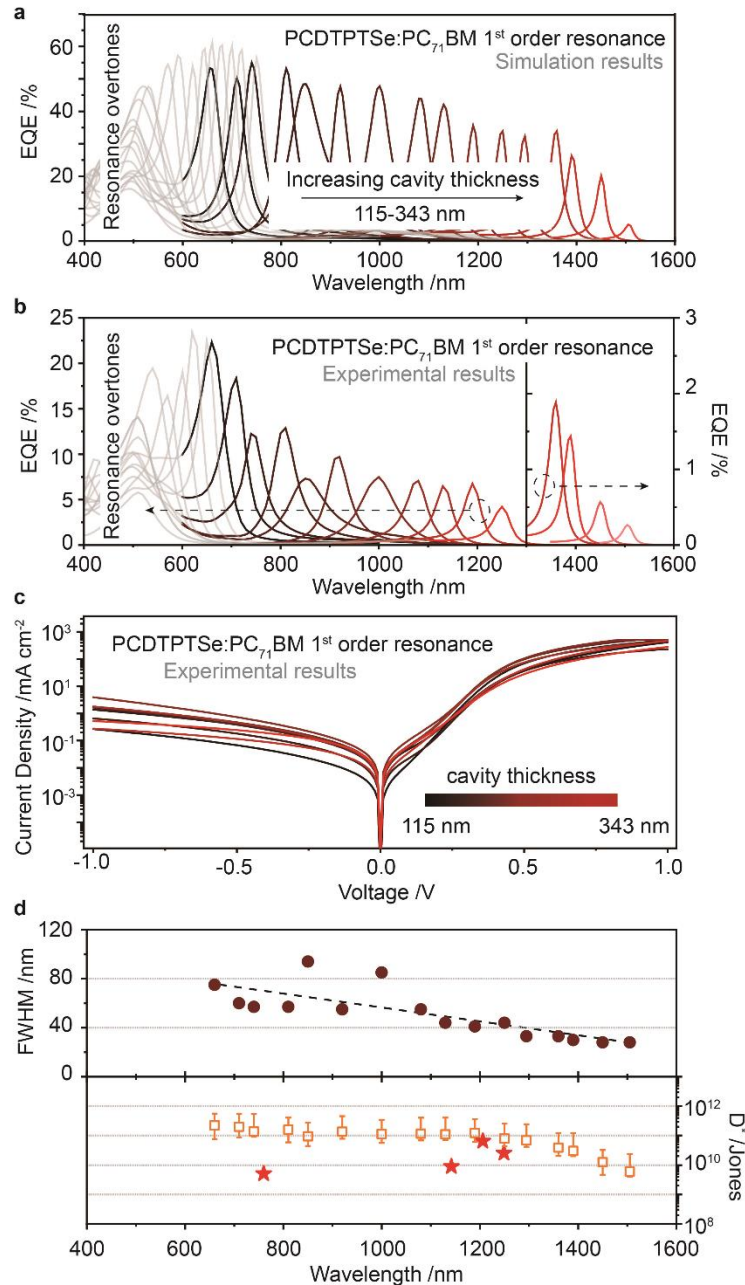


Figure 2 (a) TM simulated and (b) experimentally obtained EQE spectra for the cavity photodetectors based on PCDTPTSe:PC<sub>71</sub>BM with first order resonances: Increasing the cavity thickness by varying the thicknesses of the active layer and the interlayers enables a tunable spectral response in the wavelength range of 660–1510 nm. (c) Dark  $J$ - $V$  curves, (d) FWHM and calculated specific  $D^*$  (square) for the cavity photodetectors based on PCDTPTSe:PC<sub>71</sub>BM.  $D^*$  (star) values calculated from measured noise current for some of the devices are also indicated in the lower panel of (d). The noise current spectra are provided in Figure S10 (SI).

With this in mind, we designed a new conjugated polymer, PCDTPTSe, based on the idea that the atomic substitution of S by Se in conjugated polymers can lead to a reduced optical gap<sup>35,36</sup>. The chemical structure of PCDTPTSe is given in Figure 1c, and the synthetic route is provided in the SI-1. We find that the energy of the bandgap of PCDTPTSe is reduced by 0.15 eV, as compared to that of PCDTPT<sup>37</sup> in which [1,2,5]thiadiazolo[3,4-*c*]pyridine instead of [1,2,5]selenadiazolo[3,4-*c*]pyridine is used to form the conjugated backbone (Figure S4, SI). Importantly, the reduced bandgap of PCDTPTSe is associated with a lowered absorption coefficient within the optimal range for cavity enhancement in the NIR region. Using blends of PCDTPTSe and PC<sub>71</sub>BM we expect, based on Figure 1b, to achieve a tunable spectral response in the broad wavelength range of 600–1450 nm, while achieving FWHM <100 nm and EQE >5%.

To better predict the optical performance of the cavity photodetectors based on PCDTPTSe:PC<sub>71</sub>BM, TM simulations are carried out using the measured optical constants of PCDTPTSe:PC<sub>71</sub>BM. Because MoO<sub>3</sub> absorbs wavelengths longer than 1000 nm, the thickness of the MoO<sub>3</sub> interlayer is kept to a small value (10 nm) to minimize parasitic losses in this layer. On the other hand, the thicknesses of the ZnO interlayer and the active layer are optimized for each (first-order) resonance wavelength. As shown in Figure 2a, the total cavity thickness *L* is expected to vary from 115 to 343 nm to support a resonance wavelength in the range between 660 and 1510 nm, and the predicted FWHM values and peak EQE are in the ranges of 25–85 nm and 5–55%, respectively. Since the reflection losses are lower than 20% for most of the resonance wavelengths (Figure S5, SI), the absorption at resonance in the PCDTPTSe:PC<sub>71</sub>BM active layer and therefore EQE of the devices, is limited by parasitic absorption losses, mainly in the metal electrodes (Figure S5, SI).

Real-world cavity photodetectors are then constructed using standard fabrication procedures described in experimental section and the device architecture optimized by the TM simulations. As shown in Figure 2b, high spectral selectivity can indeed be realized experimentally for the cavity photodetectors based on PCDTPTSe:PC<sub>71</sub>BM: The lowest FWHM value achieved is 28 nm (Figure 2d), which is close to that predicted by the TM simulations. Meanwhile, tunable spectral response is achieved for a wide wavelength range (660–1510 nm). Note that the EQEs are measured for the devices under a short-circuit condition.

It is also noted that the EQEs of the cavity photodetectors are lower than that predicted by the TM simulations. The reason can partially be ascribed to the variation of the cavity thickness within the photoactive area, induced by the high roughness of the active layer surface. Atomic force microscope (AFM) images reveal that the root-mean-square (RMS) surface roughness of the active layer is about 3 nm (Figure S6), which according to TM simulations, can lead to a decrease of peak EQE value by 20–50% depending on the resonance wavelength (Figure S7). In addition, we expect

that the internal quantum efficiency (IQE) of the cavity photodetectors based on the low-bandgap PCDTPTSe:PC<sub>71</sub>BM system is rather low, since the IQE of a non-cavity enhanced photodetector based on PCDTPTSe:PC<sub>71</sub>BM and an ITO bottom electrode is in the range of only 10–40%, depending on the thickness of the active layer. A likely reason for the limited IQE is the fast recombination loss of photogenerated charge carriers: ECT of the active layer based on the low-bandgap absorber is very low, thus vibrational coupling between the excited CT state and the ground states is expected to be strong in the active layer, leading to the fast recombination losses of charge carriers.<sup>29</sup> This problem has been commonly observed for optoelectronic devices based on organic blends with small *E*<sub>CT</sub>.<sup>29,38,39</sup> However, it should be noted that the EQE achieved using PCDTPTSe is much higher than that of previously reported cavity photodetectors based on CT state absorption operating in a similar wavelength range (>1000 nm).<sup>23,28</sup> In Table S1 (SI), the performance of the cavity detectors constructed in this work is compared to that of the cavity NIR organic photo detectors reported in the literature. It should also be noted that the response

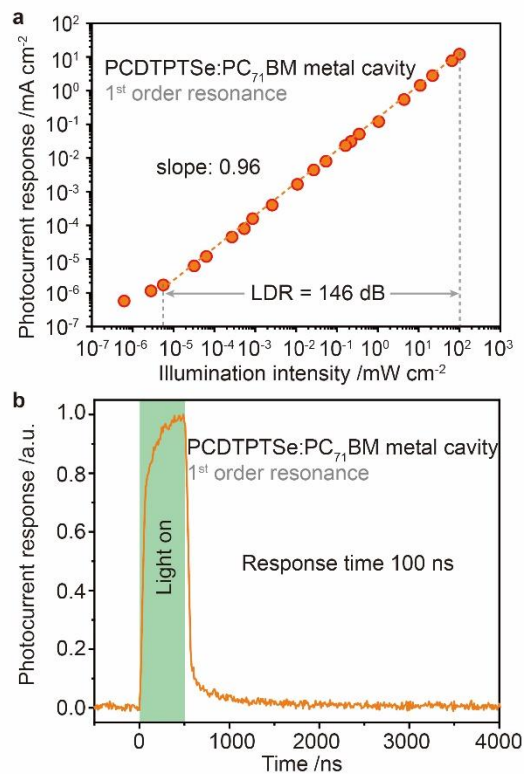


Figure 3 (a) Steady state photocurrent response of a cavity photodetector based on PCDTPTSe:PC<sub>71</sub>BM, plotted as a function of illumination intensity. The photodetector is excited at the resonance wavelength (710 nm). (b) Transient photocurrent response of the cavity photodetector measured with an illumination intensity of 100 mW cm<sup>-2</sup>. The 90–10% signal fall time is used to represent the detector response time. Both the steady state and the transient measurements are performed at a short-circuit condition and the photoactive area of the cavity photodetector is 0.04 cm<sup>2</sup>.

wavelength of the cavity photodetector can be extended to over 1600 nm (Figure S8, SI), although EQE of the cavity photodetector is further reduced because of the low absorption coefficient of PCDTPTSe in that range.

Electrical properties of the cavity photodetectors based on PCDTPTSe are characterized by the dark current density-voltage ( $J$ - $V$ ) measurements (Figure 2c) ( $J$ - $V$  curves measured under illumination are provided in Figure S9, SI). We find that the characteristics of the dark  $J$ - $V$  curves of the cavity photodetectors depend on the thickness of the active layer and the ZnO interlayer: For the best performing device, the  $J$ - $V$  curve can be fitted by a diode equation with an ideality factor of 1.6 for the low bias voltage regime. This indicates that the dark current is low, dominated by the diode saturation current.

An accurate determination of the most important figure-of-merit, the  $D^*$ , requires a direct measurement of the noise current, and to increase  $D^*$ , the device geometry, such as the shape of the electrodes, the photoactive area, etc., must be optimized for a truly reduced noise current, which is beyond the scope of this work. Instead, we first calculate an upper limit for  $D^*$ , using the method described in reference taking into account thermal noise at zero voltage bias.<sup>40</sup> As presented in Figure 2d, the calculated  $D^*$  of the cavity photodetectors based on PCDTPTSe can be as high as  $2 \times 10^{11}$  Jones, considerably better than that of the previously

reported organic photodetectors operating in the similar wavelength range.<sup>23,28</sup> In fact, the  $D^*$  of the cavity photodetectors presented in this work is comparable to that of some of the commercially available inorganic photodetectors based on Ge and PbS, operated at room temperature in the NIR wavelength range, but lacking in spectral selectivity.<sup>30,31</sup>

We also measured noise current for a set of cavity detectors with different resonant wavelengths, using the method described in the literatures<sup>41,42</sup> (Figure S10 and Figure S11, SI), and values for  $D^*$  calculated from the noise current are about 10 times lower than that estimated from the dark  $J$ - $V$  curves (Figure 2d), similar to that observed for non-cavity enhanced organic photodetectors with broadband spectral response.<sup>40</sup>

To evaluate the performance of the cavity photodetector under a wide range of illumination intensity, crucial for most photodetector applications, for instance, illumination meters, imaging, etc., the detector linear dynamic range (LDR) is measured. As shown in Figure 3a, the photocurrent response of a cavity photodetector based on PCDTPTSe is plotted as a function of irradiance, and the photocurrent generated by exciting at the resonance wavelength is found to be linear for over 7 orders of magnitude, suggesting that the LDR of the photodetector is at least 140 dB ( $20 \log$

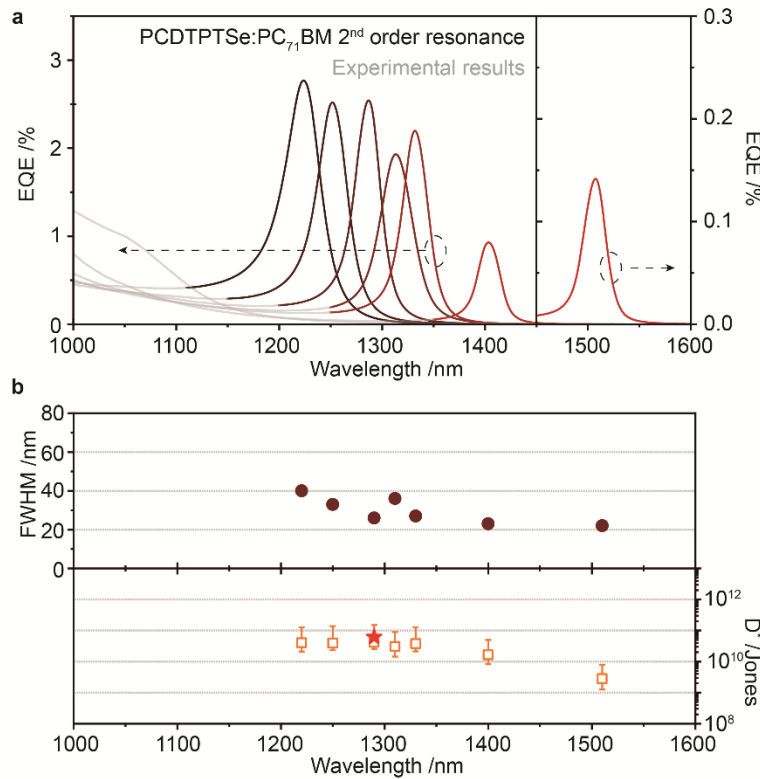


Figure 4 (a) Experimentally obtained EQE spectra for the cavity photodetectors based on PCDTPTSe:PC<sub>71</sub>BM with second-order resonances. (b) FWHM and calculated specific  $D^*$  (square) for the photodetectors based on PCDTPTSe:PC<sub>71</sub>BM.  $D^*$  (star) value calculated from measured noise current for the cavity detector with a resonance wavelength at 1300 nm is also indicated in the lower panel of (b). The noise current spectrum is provided in Figure S11 (SI).

( $I_{max}/I_{min}$ )), comparable to that of typical organic or inorganic photodetectors.<sup>40,43</sup>

The response time of the cavity photodetector is also measured to demonstrate the potential of the cavity device concept for constructing diode-array spectrometers requiring a fast readout. As shown in Figure 3b, a fall time signal (from 90% to 10%) of only 100 ns is recorded for the photocurrent response of a cavity photodetector under a short-circuit condition (cavity thickness = 133 nm, active area = 0.04 cm<sup>2</sup>), which is comparable to typical organic photodetectors reported in the literature.<sup>4,23</sup> We also note that the response time of the cavity detectors is independent of the cavity thickness (Figure S12, SI), suggesting that the response time is limited by charge carrier transit time.<sup>44</sup>

Moving to a higher-order resonance using a thicker active or spacer layer can potentially lead to reduced FWHM and improved EQE.<sup>20</sup> Such a strategy is also evaluated in this work for the cavity photodetectors based on PCDTPTSe. TM modeling (Figure S13, SI) suggests that the impact of the resonance order is mainly on the spectral selectivity. Indeed, the FWHM of the cavity photodetectors is further reduced

EQEs of the cavity photodetectors with active layer thicknesses moving the second-order resonances in the range of 1200–1550 nm are lower, compared to those with first-order resonances. This could be ascribed to the requirement of the very thick ZnO spacer (over 400 nm): The use of the too-thick ZnO spacer is expected to lead to significantly reduced charge carrier extraction efficiency, thus limits the performance of the cavity photodetector.

To evaluate the dependence of the spectral response of the cavity detectors on the angle of light incidence, EQEs of the devices are measured as a function of the angle of incidence, relative to the substrate normal. As shown in Figure S14 (SI), the peak positions of the response spectrum shift to short wavelengths with increased angle of incidence. This is expected as the narrowband spectral response is realized based on optical interferences.

To demonstrate the potential of the organic cavity photodetectors based on the low-bandgap polymer for NIR spectroscopic applications, a series of photodetectors with varied response wavelengths in the range of 660–1600 nm is selected and assembled into a miniature spectrometer, as indicated in Figure 5a. Note that all PCDTPTSe-based cavity

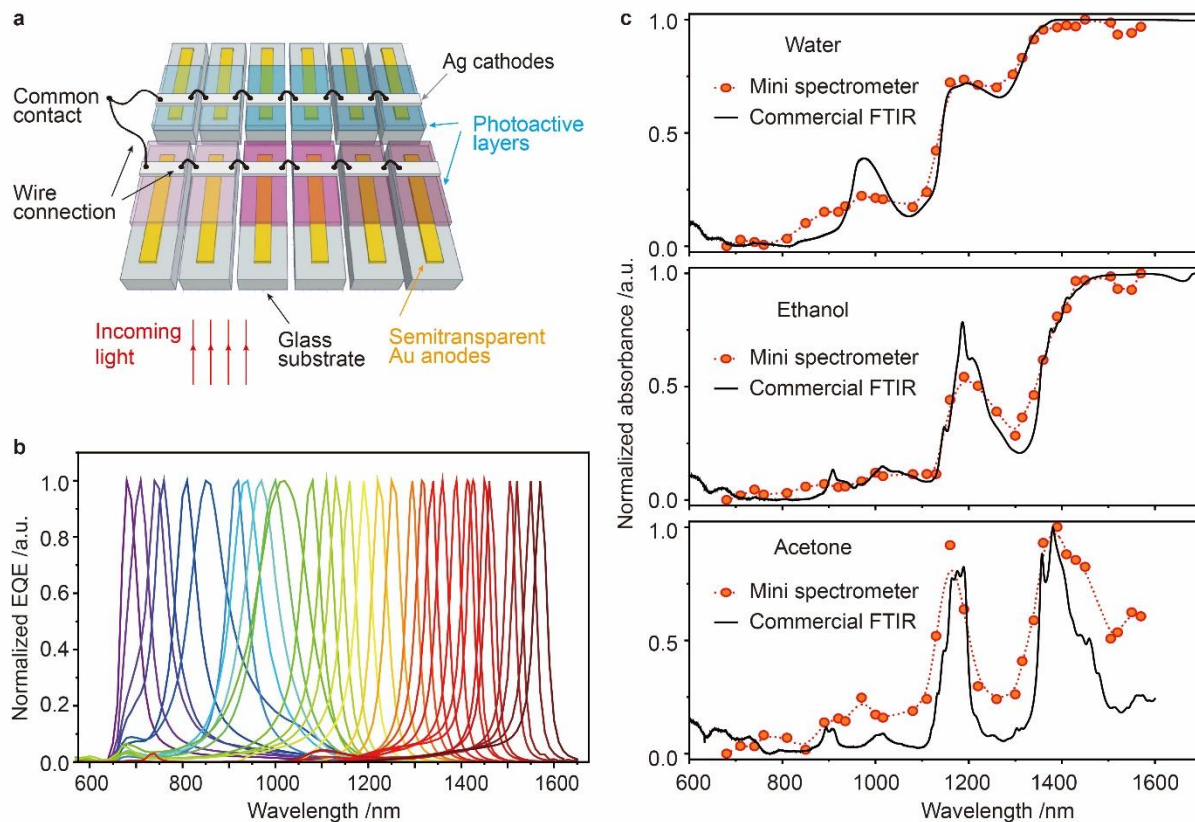


Figure 5(a) Schematic for the device architecture of the miniature spectrometer based on an array of cavity photodetectors based on PCDTPTSe:PC<sub>71</sub>BM. (b) Normalized EQE spectra of the cavity photodetectors used for the miniature spectrometer. (c) Absorption spectra of water, ethanol, and acetone measured using the miniature spectrometer, compared to the spectra measured with a commercial Fourier transform infrared spectrometer.

to 22 nm in experiments, moving to the second-order resonances (Figure 4). Nevertheless, due to lower IQE, the

photodetectors have a response in the visible spectral region for wavelengths shorter than 600 nm. This is due to

the presence of higher-order resonances which limits the free spectral range of wavelength tuning. The parasitic photocurrent in the visible wavelength range can be simply filtered out by an additional organic photo-absorbing layer acting as a filter in front of each cavity photodetector, making the photoresponse of each cavity detector truly monochromatic. The impact of an organic filter on the response spectrum of a cavity photodetector is shown in Figure S15 (SI), and the response spectra of the cavity photodetectors used to build the miniature spectrometer are presented in Figure 5b.

The miniature spectrometer based on organic cavity photodetectors is evaluated as a sensor able to record the NIR fingerprint of several common solvents. As shown in Figure 5c, using a halogen lamp as an external light source, we successfully resolved the characteristic absorption features of water, ethanol, and acetone.

## CONCLUSIONS

In summary, we show that cavity photodetectors based on organic absorbers are particularly promising, because the optical properties of organic materials can be tuned to meet the criteria required by the cavity device concept. As an example, we demonstrate that the replacement of S by Se in a conjugated polymer leads to a significantly reduced optical gap and a lowered absorption coefficient. Thus, using this newly synthesized low-bandgap polymer, PCDTPTSe, we successfully constructed cavity organic photodetectors operating in the NIR spectrum with a tunable spectral response in the wavelength range between 660–1510 nm, an FWHM down to 22 nm, and peak EQEs up to 20%. In order to increase the device responsivity and extend the wavelength range, further optimizations regarding the energetics of the active materials and the processing conditions for constructing the cavity devices are needed. Nevertheless, in this work, we realized calculated  $D^*$  values over  $10^{11}$  Jones, and measured  $D^*$  in the range of  $10^{10}$  to  $10^{11}$  Jones, comparable to that of some commercial broadband photodetectors, operating in a similar wavelength range. Finally, a proof-of-concept miniature NIR spectrometer was constructed by a series of PCDTPTSe-based cavity photodetectors, and we showed that the resolution of the miniature spectrometer was sufficiently high for detecting solvents, such as water, ethanol, or acetone.

## EXPERIMENTAL SECTION

**Synthesis:** The details for synthesis of PCDTPTSe are provided in Supporting Information.

**Device fabrication:** PC<sub>71</sub>BM was purchased from Solenne B.V. The ZnO precursor was prepared by dissolving zinc acetate dihydrate (1 g, Sigma-Aldrich), and ethanolamine (0.28 g, Sigma-Aldrich) in 2-methoxyethanol (10 mL, Sigma-Aldrich). The precursor solution was stirred for 12 h and filtered prior to use. The cavity photodetectors were constructed on cleaned glass substrates. The substrates

were ultrasonicated in detergent for 15 min, and then cleaned by TL-1 treatment (NH<sub>3</sub>·H<sub>2</sub>O: H<sub>2</sub>O<sub>2</sub>: H<sub>2</sub>O = 1:1:5, vol ratio, at 80 °C for 2 h). Au electrodes (30 nm) were thermally evaporated onto the cleaned glass substrates using a shadow mask in a vacuum chamber ( $6 \times 10^{-6}$  mbar) at a rate of 2.5 Å/s. The ZnO spacer layers were spin-coated onto the Au electrodes, using the ZnO precursor solution, and they were annealed at 200 °C for 30 min. Thick ZnO spacer layers were realized by depositing multiply ZnO layers on top of each other. The active layers were spin-coated onto the ZnO-coated substrates from a chlorobenzene solution (2% DIO, vol, PCDTPTSe:PC<sub>71</sub>BM = 1:3, weight ratio) in a nitrogen-filled glovebox. The concentration of the active layer solution is varied in the range between 12.5 and 40 mg/mL to achieve different cavity thicknesses. Finally, 10 nm thick MoO<sub>3</sub> and 120 nm thick Ag were thermally evaporated on top of the active layer. The photoactive area of the cavity photodetectors was determined by the overlapping area between the Ag and the Au electrodes (0.04 cm<sup>2</sup>).

**Device characterization:** EQE spectra were measured using a chopped and collimated halogen lamp as the light source coupled with a monochromator (Newport CS260). The chopping frequency was 173 Hz. The photoresponse signals from the cavity detectors were amplified by a pre-amplifier (Stanford instrument SR570) and recorded by a lock-in amplifier (Stanford instrument SR830). The spectral photon flux from the monochromator was calibrated with a Si detector and an InGaAs detector. Reflectance and transmittance spectra of the thin-films were measured by a PerkinElmer UV-vis-NIR spectrometer (model Lambda 950), and the optical constants of the materials used for the TM simulations were determined by spectroscopic ellipsometry (J. A. Woolam M-2000). Current density-voltage ( $J$ - $V$ ) characteristic curves were measured with a Keithley 2400 Source-Meter. AFM images were taken by using an Asylum Research MFP-3D Bio Instrument. Linear dynamic range of the cavity photodetectors was measured using a set of neutral density filters, a supercontinuum laser (model SC400 from NKT photonics), and a Keithley 2450 Source-Meter. The transient photocurrent response was measured with an LED lamp (on/off time  $\approx$  10 ns), driven by a function generator (Tektronix AFG3000), and the signals were recorded with an oscilloscope (Tektronix, MDO4104C). Noise spectral density of the devices was obtained by fast Fourier transform of the dark current versus time ( $I$ - $t$ ) curves, which were recorded with a semiconductor analyzer (B1500A, Keysight).  $I$ - $t$  curves of the devices were recorded for 40 s with a time interval of 100 ms at zero voltage. All devices were measured at room temperature on a probe station (HCS621G, Instec) with triax cables.

## ASSOCIATED CONTENT

### Supporting Information

The details for synthesis of PCDTPTSe and additional figures and tables. This material is available free of charge via the Internet at <http://pubs.acs.org>.

## AUTHOR INFORMATION

### Corresponding Authors

\*Jun Huang - State Key Laboratory for Modification of Chemical Fibers and Polymer Materials, Center for Advanced Low-dimension Materials, College of Materials Science and Engineering, Donghua University, Shanghai 201620, China; Email: [huangi@dhu.edu.cn](mailto:huangi@dhu.edu.cn)

\*Zaifei Ma - State Key Laboratory for Modification of Chemical Fibers and Polymer Materials, Center for Advanced Low-dimension Materials, College of Materials Science and Engineering, Donghua University, Shanghai 201620, China; Email: [mazaiifei@dhu.edu.cn](mailto:mazaiifei@dhu.edu.cn)

\*Zheng Tang - State Key Laboratory for Modification of Chemical Fibers and Polymer Materials, Center for Advanced Low-dimension Materials, College of Materials Science and Engineering, Donghua University, Shanghai 201620, China; Email: [ztang@dhu.edu.cn](mailto:ztang@dhu.edu.cn)

### Authors

Jinjin Yang - State Key Laboratory for Modification of Chemical Fibers and Polymer Materials, Center for Advanced Low-dimension Materials, College of Materials Science and Engineering, Donghua University, Shanghai 201620, China

Ruiming Li - Key Lab of Artificial Micro- and Nano-structures of Ministry of Education of China, School of Physics and Technology, Wuhan University, Wuhan 430072, China

Hui Li - State Key Laboratory for Modification of Chemical Fibers and Polymer Materials, Center for Advanced Low-dimension Materials, College of Materials Science and Engineering, Donghua University, Shanghai 201620, China

Bin Sun - State Key Laboratory for Modification of Chemical Fibers and Polymer Materials, Center for Advanced Low-dimension Materials, College of Materials Science and Engineering, Donghua University, Shanghai 201620, China

Qianqian Lin - Key Lab of Artificial Micro- and Nano-structures of Ministry of Education of China, School of Physics and Technology, Wuhan University, Wuhan 430072, China

Ming Wang - State Key Laboratory for Modification of Chemical Fibers and Polymer Materials, Center for Advanced Low-dimension Materials, College of Materials

Science and Engineering, Donghua University, Shanghai 201620, China

Koen Vandewal - Institute for Materials Research (IMO-IMOMEC), Hasselt University, Wetenschapspark 1, B-3590 Diepenbeek, Belgium

## NOTES

The authors declare no competing financial interest.

## ACKNOWLEDGMENTS

The work was financially supported by the National Natural Science Foundation of China (NSFC, Grant No. 51973031, 51933001, 52073056) and Shanghai Pujiang program (Grant No. 19PJ1400500). Z. Ma is grateful for the supports from the Natural Science Foundation of Shanghai (Grant No. 19ZR1401400). Z. Ma and J. Huang acknowledges the Fundamental Research Funds for the Central Universities (Grant No. 2232021A09, 20D128502). K. Vandewal acknowledges the European Research Council (ERC, grant agreement 864625) for funding.

## REFERENCES

- (1) Bacon, C. P.; Mattley, Y.; DeFrece, R. Miniature Spectroscopic Instrumentation: Applications to Biology and Chemistry. *Rev. Sci. Instrum.* **2004**, *75* (1), 1–16.
- (2) Arquer, F. P. G. de; Armin, A.; Meredith, P.; Sargent, E. H. Solution-Processed Semiconductors for next-Generation Photodetectors. *Nat. Rev. Mater.* **2017**, *2* (3), 1–17.
- (3) Yu, G.; Gao, J.; Hummelen, J. C.; Wudl, F.; Heeger, A. J. Polymer Photovoltaic Cells: Enhanced Efficiencies via a Network of Internal Donor-Acceptor Heterojunctions. *Science* **1995**, *270* (5243), 1789–1791.
- (4) Baeg, K.-J.; Binda, M.; Natali, D.; Caironi, M.; Noh, Y.-Y. Organic Light Detectors: Photodiodes and Phototransistors. *Adv. Mater.* **2013**, *25* (31), 4267–4295.
- (5) Vuuren, R. D. J.; Armin, A.; Pandey, A. K.; Burn, P. L.; Meredith, P. Organic Photodiodes: The Future of Full Color Detection and Image Sensing. *Adv. Mater.* **2016**, *28* (24), 4766–4802.
- (6) Chow, P. C. Y.; Someya, T. Organic Photodetectors for Next-Generation Wearable Electronics. *Adv. Mater.* **2020**, *32* (15), 1902045.
- (7) Jansen van Vuuren, R.; Johnstone, K. D.; Ratnasingam, S.; Barcena, H.; Deakin, P. C.; Pandey, A. K.; Burn, P. L.; Collins, S.; Samuel, I. D. W. Determining the Absorption Tolerance of Single Chromophore Photodiodes for Machine Vision. *Appl. Phys. Lett.* **2010**, *96* (25), 253303.
- (8) Lee, K.-H.; Lee, G. H.; Leem, D.-S.; Lee, J.; Chung, J. W.; Bulliard, X.; Choi, H.; Park, K.-B.; Kim, K.-S.; Jin, Y. W.; Lee, S.; Park, S. Y. Dynamic Characterization of Green-Sensitive Organic Photodetectors Using Nonfullerene Small Molecules: Frequency Response Based on the Molecular Structure. *J. Phys. Chem. C* **2014**, *118* (25), 13424–13431.
- (9) Han, M. G.; Park, K.-B.; Bulliard, X.; Lee, G. H.; Yun, S.; Leem, D.-S.; Heo, C.-J.; Yagi, T.; Sakurai, R.; Ro, T.; Lim, S.-J.; Sul, S.; Na, K.; Ahn, J.; Jin, Y. W.; Lee, S. Narrow-Band Organic Photodiodes for High-Resolution Imaging. *ACS Appl. Mater. Interfaces* **2016**, *8* (39), 26143–26151.
- (10) Lyons, D. M.; Armin, A.; Stolterfoht, M.; Nagiri, R. C. R.; Jansen-van Vuuren, R. D.; Pal, B. N.; Burn, P. L.; Lo, S.-C.

- Meredith, P. Narrow Band Green Organic Photodiodes for Imaging. *Org. Electron.* **2014**, *15* (11), 2903–2911.
- (11) Zhu, L.; Wang, W. S.; Yao, Z. G.; Zhang, X. Q.; Wang, Y. S. Ultraviolet Photodetectors With Narrow-Band Spectral Response Using TAPC Donor. *IEEE T. Electron Dev.* **2012**, *59* (12), 3583–3586.
- (12) Zhong, Y.; Sisto, T. J.; Zhang, B.; Miyata, K.; Zhu, X.-Y.; Steigerwald, M. L.; Ng, F.; Nuckolls, C. Helical Nanoribbons for Ultra-Narrowband Photodetectors. *J. Am. Chem. Soc.* **2017**, *139* (16), 5644–5647.
- (13) Fang, Y.; Dong, Q.; Shao, Y.; Yuan, Y.; Huang, J. Highly Narrowband Perovskite Single-Crystal Photodetectors Enabled by Surface-Charge Recombination. *Nature Photon.* **2015**, *9* (10), 679–686.
- (14) Armin, A.; Jansen-van Vuuren, R. D.; Kopidakis, N.; Burn, P. L.; Meredith, P. Narrowband Light Detection via Internal Quantum Efficiency Manipulation of Organic Photodiodes. *Nat. Commun.* **2015**, *6* (1), 6343.
- (15) El-Batawy, Y.; Mohammedy, F. M.; Deen, M. J. 13 - Resonant Cavity Enhanced Photodetectors: Theory, Design and Modeling. In *Photodetectors*; Nabet, B., Ed.; Woodhead Publishing, **2016**; pp 415–470.
- (16) Ünlü, M. S.; Emsley, M. K.; Dosunmu, O. I.; Muller, P.; Leblebici, Y. High-Speed Si Resonant Cavity Enhanced Photodetectors and Arrays. *J. Vac. Sci. Technol.* **2004**, *22*, 781–787.
- (17) Vahala, K. J. Optical Microcavities. *Nature* **2003**, *424* (6950), 839–846.
- (18) Lupton, J. M.; Koeppe, R.; Müller, J. G.; Feldmann, J.; Scherf, U.; Lemmer, U. Organic Microcavity Photodiodes. *Adv. Mater.* **2003**, *15* (17), 1471–1474.
- (19) An, K. H.; O'Connor, B.; Pipe, K. P.; Shtein, M. Organic Photodetector with Spectral Response Tunable across the Visible Spectrum by Means of Internal Optical Microcavity. *Org. Electron.* **2009**, *10* (6), 1152–1157.
- (20) Ünlü, M. S.; Strite, S. Resonant Cavity Enhanced Photonic Devices. *J. Appl. Phys.* **1995**, *78* (2), 607–639.
- (21) Kishino, K.; Unlu, M. S.; Chyi, J.-I.; Reed, J.; Arsenault, L.; Morkoc, H. Resonant Cavity-Enhanced (RCE) Photodetectors. *IEEE J. Quantum Electron.* **1991**, *27* (8), 2025–2034.
- (22) Yazmaciyan, A.; Meredith, P.; Armin, A. Cavity Enhanced Organic Photodiodes with Charge Collection Narrowing. *Adv. Opt. Mater.* **2019**, *7* (8), 1801543.
- (23) Tang, Z.; Ma, Z.; Sánchez-Díaz, A.; Ullbrich, S.; Liu, Y.; Siegmund, B.; Mischok, A.; Leo, K.; Campoy-Quiles, M.; Li, W.; Vandewal, K. Polymer:Fullerene Bimolecular Crystals for Near-Infrared Spectroscopic Photodetectors. *Adv. Mater.* **2017**, *29* (33), 1702184.
- (24) Wang, J.; Ullbrich, S.; Hou, J.-L.; Spoltore, D.; Wang, Q.; Ma, Z.; Tang, Z.; Vandewal, K. Organic Cavity Photodetectors Based on Nanometer-Thick Active Layers for Tunable Monochromatic Spectral Response. *ACS. Photo.* **2019**, *6* (6), 1393–1399.
- (25) Vandewal, K.; Albrecht, S.; Hoke, E.; Graham, K.; Widmer, J.; Douglas, J.; Schubert, M.; Mateker, W.; Bloking, J.; Burkhard, G.; Sellinger, A.; Fréchet, J.; Amassian, A.; Riede, M.; McGehee, M.; Neher, D.; Salbeck, A. Efficient Charge Generation by Relaxed Charge-Transfer States at Organic Interfaces. *Nature Mater.* **2013**, *13* (1), 63–68.
- (26) Vandewal, K. Interfacial Charge Transfer States in Condensed Phase Systems. *Annu. Rev. Phys. Chem.* **2016**, *67* (1), 113–133.
- (27) Kaiser, C.; Schellhammer, K. S.; Benduhn, J.; Siegmund, B.; Tropicano, M.; Kublitski, J.; Spoltore, D.; Panhans, M.; Zeika, O.; Ortmann, F.; Meredith, P.; Armin, A.; Vandewal, K. Manipulating the Charge Transfer Absorption for Narrowband Light Detection in the Near-Infrared. *Chem. Mater.* **2019**, *31* (22), 9325–9330.
- (28) Siegmund, B.; Mischok, A.; Benduhn, J.; Zeika, O.; Ullbrich, S.; Nehm, F.; Böhm, M.; Spoltore, D.; Fröb, H.; Körner, C.; Leo, K.; Vandewal, K. Organic Narrowband Near-Infrared Photodetectors Based on Intermolecular Charge-Transfer Absorption. *Nat. Commun.* **2017**, *8* (1), 15421.
- (29) Gielen, S.; Kaiser, C.; Verstraeten, F.; Kublitski, J.; Benduhn, J.; Spoltore, D.; Verstappen, P.; Maes, W.; Meredith, P.; Armin, A.; Vandewal, K. Intrinsic Detectivity Limits of Organic Near-Infrared Photodetectors. *Adv. Mater.* **2020**, *32* (47), 2003818.
- (30) Xu, Y.; Lin, Q. Photodetectors Based on Solution-Processable Semiconductors: Recent Advances and Perspectives. *Appl. Phys. Rev.* **2020**, *7* (1), 011315.
- (31) Zeller, J. W.; Efstathiadis, H.; Bhowmik, G.; Haldar, P.; Dhar, N. K.; Lewis, J.; Wijewarnasuriya, P.; Puri, Y. R.; Sood, A. K. Development of Ge PIN Photodetectors on 300 Mm Si Wafers for Near-Infrared Sensing. *Int. J. Eng. Res. Technol.* **2015**, *8*, 23–33.
- (32) Pettersson, L. A. A.; Roman, L. S.; Inganäs, O. Modeling Photocurrent Action Spectra of Photovoltaic Devices Based on Organic Thin Films. *J. Appl. Phys.* **1999**, *86* (1), 487–496.
- (33) Ma, R.; Liu, T.; Luo, Z.; Guo, Q.; Xiao, Y.; Chen, Y.; Li, X.; Luo, S.; Lu, X.; Zhang, M.; Li, Y.; Yan, H. Improving Open-Circuit Voltage by a Chlorinated Polymer Donor Endows Binary Organic Solar Cells Efficiencies over 17%. *Sci. China Chem.* **2020**, *63* (3), 325–330.
- (34) Zhao, W.; Qian, D.; Zhang, S.; Li, S.; Inganäs, O.; Gao, F.; Hou, J. Fullerene-Free Polymer Solar Cells with over 11% Efficiency and Excellent Thermal Stability. *Adv. Mater.* **2016**, *28* (23), 4734–4739.
- (35) Gibson, G. L.; McCormick, T. M.; Seferos, D. S. Atomistic Band Gap Engineering in Donor–Acceptor Polymers. *J. Am. Chem. Soc.* **2012**, *134* (1), 539–547.
- (36) Hollinger, J.; Gao, D.; Seferos, D. S. Selenophene Electronics. *Isr. J. Chem.* **2014**, *54* (5–6), 440–453.
- (37) Ying, L.; Hsu, B. B. Y.; Zhan, H.; Welch, G. C.; Zalar, P.; Perez, L. A.; Kramer, E. J.; Nguyen, T.-Q.; Heeger, A. J.; Wong, W.-Y.; Bazan, G. C. Regioregular Pyridal[2,1,3]Thiadiazole  $\pi$ -Conjugated Copolymers. *J. Am. Chem. Soc.* **2011**, *133* (46), 18538–18541.
- (38) Verstraeten, F.; Gielen, S.; Verstappen, P.; Kesters, J.; Georgitzikis, E.; Raymakers, J.; Cheyns, D.; Malinowski, P.; Daenen, M.; Lutsen, L.; Vandewal, K.; Maes, W. Near-Infrared Organic Photodetectors Based on Bay-Annulated Indigo Showing Broadband Absorption and High Detectivities up to 1.1 Mm. *J. Mater. Chem. C* **2018**, *6* (43), 11645–11650.
- (39) Verstraeten, F.; Gielen, S.; Verstappen, P.; Raymakers, J.; Penxten, H.; Lutsen, L.; Vandewal, K.; Maes, W. Efficient and Readily Tuneable Near-Infrared Photodetection up to 1500 Nm Enabled by Thiadiazoloquinoxaline-Based Push–Pull Type Conjugated Polymers. *J. Mater. Chem. C* **2020**, *8* (29), 10098–10103.
- (40) Armin, A.; Hamsch, M.; Kim, I. K.; Burn, P. L.; Meredith, P.; Namdas, E. B. Thick Junction Broadband Organic Photodiodes. *Laser & Photonics Rev.* **2014**, *8* (6), 924–932.
- (41) Lan, Z.; Lei, Y.; Chan, W. K. E.; Chen, S.; Luo, D.; Zhu, F. Near-Infrared and Visible Light Dual-Mode Organic Photodetectors. *Sci. Adv.* **2020**, *6* (5), eaaw8065.
- (42) Lin, Q.; Armin, A.; Burn, P. L.; Meredith, P. Filterless Narrowband Visible Photodetectors. *Nature Photon.* **2015**, *9* (10), 687–694.
- (43) Guo, F.; Xiao, Z.; Huang, J. Fullerene Photodetectors with a Linear Dynamic Range of 90 DB Enabled by a Cross-

---

Linkable Buffer Layer. *Adv. Opt. Mater.* **2013**, *1* (4), 289–294.

- (44) Lan, Z.; Lau, Y. S.; Wang, Y.; Xiao, Z.; Ding, L.; Luo, D.; Zhu, F. Filter-Free Band-Selective Organic Photodetectors. *Adv. Opt. Mater.* **2020**, *8* (24), 2001388.

---

## Table of Contents

**Title:** Cavity-Enhanced Near-Infrared Organic Photodetectors Based on A Conjugated Polymer Containing [1,2,5]Selenadiazolo[3,4-c]pyridine

Cavity-enhanced narrowband photodetectors with different spectral responses in the wavelength range of 660-1510 nm are demonstrated using a low-bandgap polymer absorber with relatively low absorption coefficients in the near-infrared spectral range. This enables the construction of a miniaturized spectrometer free of dispersive optics by assembling the cavity photodetectors into an array.

